Optimizing Vertical and Lateral Waveguides of kW-Class Laser Bars for Higher Peak Power, Efficiency and Lateral Beam Quality

Md. Jarez Miah 🔘 , *Member, IEEE*, Anisuzzaman Boni, Seval Arslan, Dominik Martin, Pietro Della Casa 🔘 , and Paul Crump 🔘 , *Senior Member, IEEE*

Abstract—GaAs-based, highly-efficient, kW-class, 1-cm laser bars with high peak power P_{opt} and improved beam quality in quasi-continuous-wave mode are presented. The use of an extreme-triple-asymmetric (ETAS) epitaxial layer structure diminishes power saturation of high-power bars at high driving current. The resulting ETAS bars with 4 mm cavity produce a record 1.9 kW peak power, limited by available current supply, with a maximum power conversion efficiency $\eta_E = 67\%$ at $T_{HS} = 25\ °C$ heat-sink temperature. Both P_{opt} and η_E have been increased further by operating the bars at $T_{HS} = -70\ °C$. Sub-zero operation raises the P_{opt} to 2.3 kW and the maximum η_E to 74%. A second configuration of ETAS bars with optimized lateral layout is further realized to obtain narrow lateral beam divergence θ up to 2 kA driving current, without sacrificing P_{opt} and η_E. A 2–3° lower θ (95% power level) is observed over a wide operating range at room temperature. A high degree of polarization is also maintained across the whole operating range.

Index Terms—Beam quality, beam parameter product, diode lasers, high efficiency, high-power lasers, laser bars, near field, far field, semiconductor lasers.

I. INTRODUCTION

SEMICONDUCTOR lasers (SLs) are in high demand for many applications because of their high power, high power conversion efficiency (η_E), small size, low cost etc. GaAs-based SLs are used as sources for pumping solid-state and fiber lasers [1]. For pulse-pump applications, such laser sources are typically arranged together in a stack and operated under quasi-continuous-wave (QCW) mode. QCW laser bars providing more than $P_{opt} = 1$ kW peak power have been realized both in single bar [2] and stack configuration [3]. Power scaling is possible by integrating several active regions using tunnel junction (TJ). A bar peak power as high as 1.9 kW at $T_{HS} = 25\ °C$ heat-sink temperature was achieved, where two laser structures were vertically integrated [4]. However, such TJ-based bars suffer from intrinsically poor vertical beam quality, $\sim$2x diffraction limited, unless special measures are used [5].

The highest peak power per bar from a single junction at $T_{HS} \sim 25\ °C$ to date is reported in [6]. The QCW laser bars with $L = 6$ mm cavity length yield 1.5 kW peak power with maximum $\eta_E = 63\%$. Even higher peak power of 2 kW and a maximum $\eta_E = 77\%$ was achieved from QCW bars with $L = 4$ mm, but at a lower $T_{HS} = -70\ °C$ [7]. A further improvement in the power (per bar, preferably with $L \leq 4$ mm) and η_E is needed to reduce the system cost ($/W). The bars presented in [6], [7] are based on asymmetric large optical cavity (ASLOC) structures which produce nearly symmetric vertical mode distributions in both sides of the active region. The mode extension into a relatively thick p-doped waveguide (p-WG) causes either high optical loss through free-carrier absorption, or high resistance. The structures also suffer from excessive power saturation due to high bias-driven carrier leakage [8]. Thus, the maximum P_{opt} and η_E at high operating current (I_{opt}) are limited.

In this paper, we present our recently-developed single junction kW-class QCW laser bars and compare these to baseline devices. The highest performance "best practice" bars are a first-time combination of proven high performance extreme-triple-asymmetric (ETAS) epitaxial design (low power saturation) with a wide-stripe bar layout (lower edge loss for higher power) and high front facet reflectivity (reduced losses from longitudinal spatial hole burning). Their performance is assessed compared to the reference ASLOC (strong power saturation) bars, that use a narrow stripe configuration (high edge loss). Power and conversion efficiency are measured up to 2 kA at both room and sub-zero temperature, and "best practice" bars reach much higher powers than the reference material and our previous work. We also investigate the impact of lateral-waveguiding mechanism on the beam quality of the laser bars up to 2 kA for the first time. We confirm experimentally that the lateral beam divergence θ and degree of polarization (DOP) are both improved up to peak current by omitting the additional lateral guiding and mechanical stress associated with etched index guiding grooves.

II. EXPERIMENTAL RESULTS

The ETAS structure presented in this paper uses a highly asymmetric epitaxial layer structure with a thin p-WG for low series resistance R_s, and optimizes the layer structure to vertically shift the lasing mode away from the p-WG layers for low
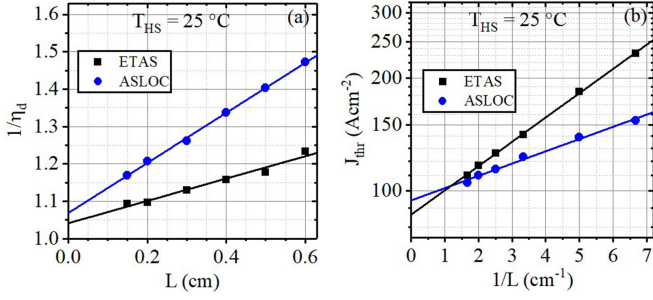
Fig. 1. (a) Inverse differential quantum efficiency $1/\eta_d$ and (b) threshold current density J_{thr} as a function of cavity length L of the BA lasers from the investigated ETAS structure (square) and the reference ASLOC structure (circle). Measurements are performed in pulsed mode at $T_{HS} = 25$ °C. Solid lines are linear fits. Note that left axis in (b) is plotted in logarithmic scale.

TABLE I
EXTRACTED INTERNAL DEVICE PARAMETERS

Structure	η_{int}	α_{int} (cm^{-1})	Γg_0 (cm^{-1})	J_{tr} (Acm^{-2})
ASLOC	0.94	0.74	15.1	89
ETAS	0.96	0.33	7.6	83

optical loss. The thin p-WG also ensures low bias-driven carrier leakage and thus low power saturation at high driving current. A sufficiently high modal gain is maintained for low threshold current. These combined lead to high P_{opt} and η_E.

ETAS based single emitters are proven to yield higher P_{opt} and η_E than the ASLOC based single emitters [9]. Here we evaluate the experimental results from 1-cm wide ETAS laser bars in comparison to kW-class reference ASLOC bars.

First, we present the internal parameters of the investigated ETAS structure. The ETAS structure, described in detail in [10] (structure with 0.54% confinement) and previously used in [11], is designed for an efficient emission at $\lambda \sim 940$ nm at $T_{HS} = 25$ °C. As a reference, we have chosen a recent efficiency optimized (unpublished) ASLOC vertical design which enabled a bar peak power over 1 kW. Both the reference ASLOC and ETAS structure contain a single InGaAs quantum well (QW) in the active region, embedded in $Al_xGa_{1-x}As$ waveguide and cladding layers. The $Al_{0.25}Ga_{0.75}As$ waveguide layers are low-doped ($< 5 \times 10^{17}$ cm^{-3}) to ensure low optical losses. Thicknesses of the p-WG of the reference ASLOC and the ETAS structure are 310 nm and 150 nm, respectively, and the effective energy barrier ΔE to electron escape into the p-waveguide is comparable at $\sim 10.4 k_B T_{HS}$ (where k_B is the Boltzmann constant and ΔE the energy difference between the conduction band and lowest confined state in the QW). Both ASLOC and ETAS structures were first processed into broad-area (BA) lasers with $w = 100$ μm stripe width and different cavity lengths (L) to obtain device parameters. Fig. 1 shows the length dependence of the differential quantum efficiency η_d and threshold current density J_{thr} of the uncoated BA lasers, with the length analysis for the ETAS design corresponding to a repeat growth and fabrication run, to the same epitaxy design used in [10], confirming reproducibility. The extracted internal parameters, i.e., internal differential quantum efficiency η_{int}, optical loss α_{int}, modal gain

factor Γg_0 and transparency current density J_{tr} are listed in Table. I. The ETAS structure shows a factor of 2.2 lower α_{int} and a slightly lower J_{tr}, but at the same time 2 times lower modal gain Γg_0 and thus higher J_{thr} (cf. Fig. 1(b)).

A. Improvement of Peak Power By Vertical Design

The reference ASLOC and ETAS structures are then processed into 1-cm wide bars. The bars from the reference ASLOC structure will be denoted as 'reference-1' bars in the following sections. The reference-1 bars contain 37 emitters with $w = 186$ μm at FF = 69% fill factor and have $L = 4$ mm. The facets are passivated and coated with reflectivity $R_f < 1\%$ at the front side and $R_r = 98\%$ at the rear side. The ETAS bars have $L = 4$ mm and consist of 20 emitters with $w = 395$ μm at FF = 79%, $R_f = 2\%$ and $R_r = 98\%$. A higher R_f is used following [12] in order to compensate for the lower gain and to minimize the enhanced longitudinal spatial hole burning effect in the ETAS structure having low Γg_0. As reported in [13], the wider stripes benefit the conversion efficiency at high operating current by reducing the volume of lossy material at the stripe edges. So here, wider stripes (395 μm vs 186 μm) are chosen for the ETAS bars for improved performance. Also, in order to avoid ring oscillations, the contacts of the emitters in the ETAS bars are sub-structured into 5 μm wide sub-stripes at 10 μm period [14]. Emitters in both ASLOC and ETAS bars are defined by ion implantation (using $^4He^+$ ions) of the contact layer. Additionally, index-guiding trenches are dry-etched ~ 10 μm away from both stripe edges of each individual emitter to achieve stable near-field distributions [15], [16]. A schematic depiction of the fully processed representative single emitters in the investigated reference-1 ASLOC and ETAS bars is given in Fig. 2. The fully processed bars are sandwiched between two expansion matched CuW heat-spreaders (0.25 mm thick) and subsequently mounted with p-side down onto a Cu block acting as a passive heat-sink. For sandwiching AuSn solder is used, while for mounting onto the Cu-block In solder is used. Fig. 3 presents output power-current-voltage (PIU) characteristics and η_E of the reference-1 ASLOC and ETAS bars at $T_{HS} = 25$ °C. The bars are characterized using $\Delta\tau = 200$ μs pulses at $f = 10$ Hz. The pulse power is measured using a thermoelectric detector which is calibrated against national standards, and voltage is measured using 4-terminal configuration. The slopes of the

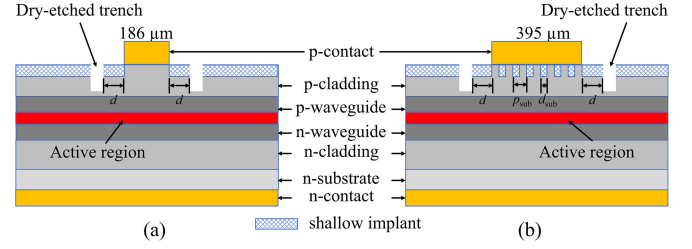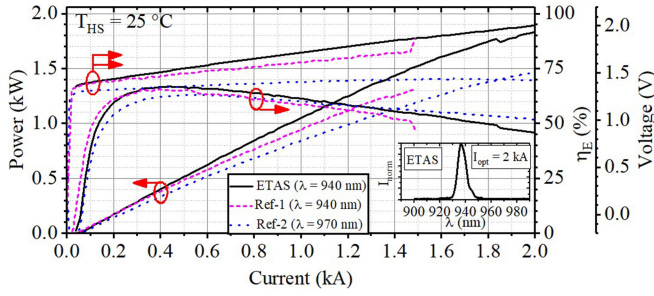

Fig. 2. Schematic depiction of the representative single emitters (SEs) in (a) the reference-1 ASLOC bar and (b) the improved ETAS bar. In the investigated bars, such SEs are repeated 37 and 20 times, respectively. The distance of the dry-etched trenches from the stripe edge $d \sim 10$ μm. Period and width of the ion implanted sub-structure in (b) are $p_{sub} = 10$ μm and $d_{sub} = 5$ μm, respectively.

Fig. 3. PIU characteristics and conversion efficiency η_E of a *reference-1* ASLOC ($L = 4$ mm, $\lambda = 940$ nm) (dashed), a *reference-2* ASLOC ($L = 6$ mm, $\lambda = 970$ nm) (dotted) and an ETAS ($L = 4$ mm, $\lambda = 940$ nm) (solid) bar in QCW mode at $T_{HS} = 25$ °C. The *reference-2* results are redrawn from [6]. (inset) Emission spectrum (I_{norm}: normalized intensity) of the ETAS bar at $I_{opt} = 2$ kA.

Fig. 4. PIU characteristics and conversion efficiency η_E of a *reference-1* ASLOC ($L = 4$ mm, $\lambda = 910$ nm) (dashed), a *reference-3* ASLOC ($L = 4$ mm, $\lambda = 940$ nm) (dotted) and an ETAS ($L = 4$ mm, $\lambda = 910$ nm) (solid) bar in QCW mode at $T_{HS} = -70$ °C. The *reference-3* results are redrawn from [7]. (inset) Emission spectrum (I_{norm}: normalized intensity) of the ETAS bar at $I_{opt} = 2$ kA.

power-current curve of both bars are similar up to $I_{opt} \sim$ 300 A, however, deviate strongly at $I_{opt} > 300$ A, with early power saturation in the ASLOC based bar. The *reference-1* bar provides a peak power $P_{opt, reference-1} = 1.31$ kW, limited by both power saturation and catastrophic optical damage (COD). The ETAS bar shows a weaker saturation, maintains a linear PI curve until very high I_{opt} and thus provides a much higher peak $P_{opt, ETAS} = 1.85$ kW. The maximum $P_{opt, ETAS}$ is limited by the available current supply of 2 kA, being the highest ever reported bar peak power for a single junction device. Although both the ETAS and *reference-1* bars provide similar maximum $\eta_E \sim 67\%$, the ETAS bar yields a higher η_E at high power levels, e.g., η_E (1.0 kW) = 62% for the ETAS bar, while 58% for the *reference-1* bar.

The performance of the ETAS bar is also compared with a second $L = 6$ mm long ASLOC bar (*reference-2*) from [6] that provided the highest previously published single junction power of $P_{opt, reference-2} = 1.5$ kW (limited by rollover) in QCW mode at $T_{HS} = 25$ °C, emitting at $\lambda \sim 970$ nm (diffraction limited vertical beam emission). The peak $P_{opt, ETAS}$ exceeds the peak $P_{opt, reference-2}$ bar by more than 23% in spite of using a shorter $L = 4$ mm. In addition, η_E values are also increased by 4%, e.g., at 1.0 kW and 1.5 kW. The kink at around 1.8 kW power arises due to an emitter failure (COD). The emission spectrum of the ETAS bar at 2 kA is presented in the inset, confirming their emission at $\lambda \sim 940$ nm at $T_{HS} = 25$ °C. We attribute increases in power to lower bias-driven carrier leakage due to the use of a thin p-WG [8].

B. Improvement of Peak Power and Efficiency By Lowering Heat-Sink Temperature

Following the suggestion in [17], both the ETAS and ASLOC bars (*reference-1*) are subsequently measured at a reduced $T_{HS} = -70$ °C to further enhance lasing performance. SLs operating at sub-zero T_{HS} are potentially promising sources for pumping large-scale solid-state lasers. At low operating temperature, material gain increases for lower threshold current and higher slope yielding higher conversion efficiency. Therefore, higher power P_{opt} and η_E are achieved. The QCW results of an ETAS and a *reference-1* ASLOC bar, sibling to the bars presented in Fig. 3, are shown in Fig. 4 at $T_{HS} = -70$ °C. Peak
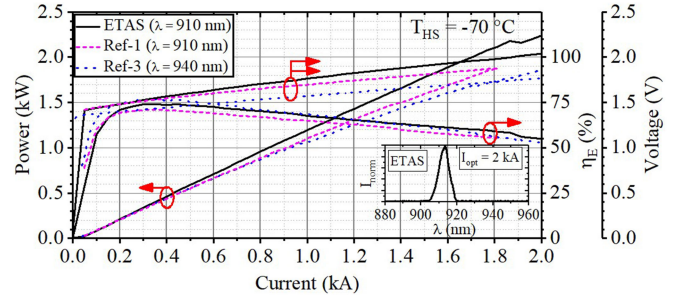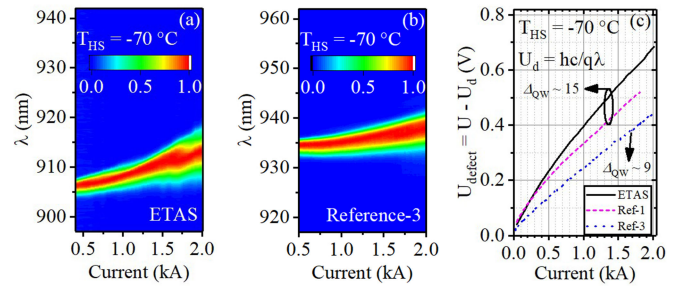

Fig. 5. False color (linearly-scaled) plot of the emission spectra of the (a) ETAS bar and (b) *reference-3* ASLOC bar presented in Fig. 4. The measurements are performed at $T_{HS} = -70$ °C. (c) Defect voltage derived from the measured voltage U across the bars in Fig. 4(c) as a function of their operating current. $\Delta_{QW} = \Delta E / K_B T_{HS}$ values are noted.

$P_{opt, ETAS}$ is increased to 2.26 kW and peak $P_{opt, reference-1}$ is increased to 1.88 kW, again limited by the available current and COD, respectively. An emitter failure within the ETAS bar produces a kink at around 2.2 kW power. The bars operate at $\lambda \sim 910$ nm at $T_{HS} = -70$ °C. The emission spectrum of the ETAS bar at 2 kA is presented in the inset of Fig. 4 and a false color plot of its emission spectra is shown in Fig. 5(a). A similar improvement is seen to that observed at $T_{HS} = 25$ °C, peak $P_{opt, ETAS}$ is $> 20\%$ higher than peak $P_{opt, reference-1}$. It is also noted that the ETAS bar provides 3% higher maximum η_E (74% vs 71%), and $\sim 5\%$ higher η_E at 1.0 kW, 1.5 kW and 1.9 kW.

QCW results of a different ASLOC bar (*reference-3*) producing best previously published P_{opt} and η_E at $T_{HS} = -70$ °C are also included from [7] in Fig. 4. The *reference-3* ASLOC bar has the same layout as *reference-1* bar. The epitaxial structure was optimized by lowering Al-contents in the p-WG to obtain highest η_E at $T_{HS} = -70$ °C. The *reference-3* bar provides a $P_{opt} = 1.9$ kW with maximum $\eta_E = 77\%$ and operates at $\lambda \sim$ 940 nm. The emission spectra of the *reference-3* bar are shown in Fig. 5(b).

Although, the maximum η_E of the ETAS bar is decreased slightly to 74% in comparison to the *reference-3* bar, η_E at $P_{opt} = 1.9$ kW is increased by 7% to 60%. It is to be noted that the ETAS structure is not specifically designed for the sub-zero operation, therefore, still better performance is achievable. The ETAS and *reference-1* structures have excessively high $\Delta E =$
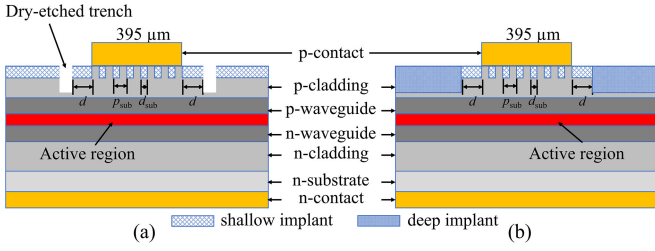
Fig. 6. Schematic depiction of the representative SEs in the investigated (a) index-guided and (b) gain-guided ETAS bar. In the bars, SEs are repeated 20 times. The distance of the dry-etched trenches in (a) and the deep implanted regions in (b) from the stripe edge $d \sim 10$ μm.

$15.2 k_B T_{HS}$ for -70 °C operation as compared to the *reference-3* ASLOC structure ($\Delta E \sim 9.2 k_B T_{HS}$), thus generating a significantly higher R_s due to capture-escape effects [7]. The ETAS structure shows a higher defect voltage $U_{defect} = U\text{-}U_d$ (where $U_d = hc/e\lambda$; h, c and e are Planck's constant, speed of light in a vacuum and electron charge, respectively) over the whole operating current range (Fig. 5(c)). This limits the maximum η_E to 74%. However, at higher I_{opt}, increase in slope efficiency and strongly reduced power saturation compensate the voltage deficiency and result in higher P_{opt} and η_E. On the other hand, in spite of having a thinner p-WG, the slightly higher R_s of the ETAS bar in comparison to the *reference-1* bar, also visible at $T_{HS} = 25$ °C in Fig. 3, is due to the thick n-doped layers and overall low and unoptimized doping concentration in the ETAS layer structure.

C. Improvement of Beam Quality By Lateral Waveguiding

As mentioned in Sect. II(A), ETAS bars presented so far have dry-etched index guides near the emitter edges which produce an effective index contrast of $\Delta n_{eff} = (0.7 \dots 1.0) \times 10^{-3}$. The resulting index-guiding allows more higher order lateral optical modes to be guided and deteriorates the lateral beam quality (i.e., increases the lateral beam divergence) at the benefit of stable near field and reduced sensitivity to thermal lensing. Following [11] to improve beam quality, a second variant of ETAS bars is processed using the same bar layout (20×395 μm, FF = 79%), but the index-guiding trenches are avoided and ion implantation (using ^{4}He$^+$ and ^{1}H$^+$ ions) depth is extended from the contact layer down into the p-cladding layer. The emitter structures within the index-guided and gain-guided ETAS bars are schematically depicted in Fig. 6. The resulting ETAS bars (containing gain-guided (GG) emitters with no intentional process-induced index-guiding) reproduce the PIU performance of the ETAS bars, presented earlier in Fig. 3, containing index-guided (IG) emitters as compared in Fig. 7, reaching 1.9 kW peak power at 2 kA.

However, due to the reduced number of optical modes guided in the laser waveguide of the GG ETAS bar, the lateral beam divergence angle is reduced, consistent with previous data for bars with 37 emitters having 186 μm wide stripes [11]. Measured far field profiles of the bars with and without index guides are shown in Fig. 8, obtained using the telescopic imaging system described in [13]. Far-field profiles are averaged across
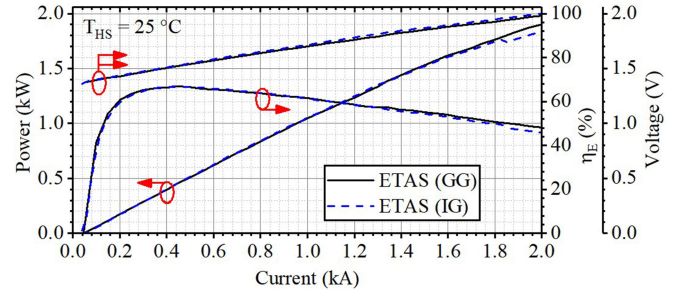

Fig. 7. PIU characteristics and conversion efficiency η_E of an ETAS laser bar containing gain-guided (GG) emitters (solid) at $T_{HS} = 25$ °C. Data for the ETAS bar with index-guided (IG) emitters (dashed) is redrawn from Fig. 3.
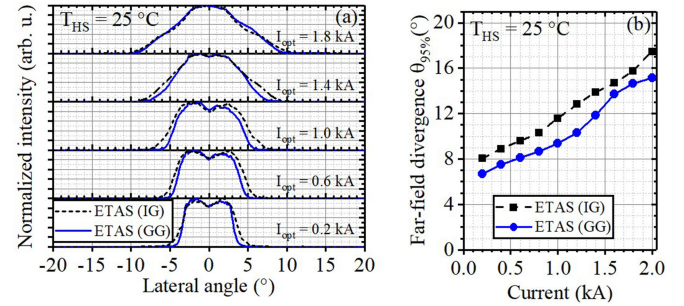

Fig. 8. (a) Far-field distributions along the lateral direction of the gain-guided (solid) and index-guided (dashed) ETAS bars at different operating currents I_{opt} at $T_{HS} = 25$ °C. (b) Far-field divergence angle containing 95% power content extracted from the distributions in (a) as a function of operating current.
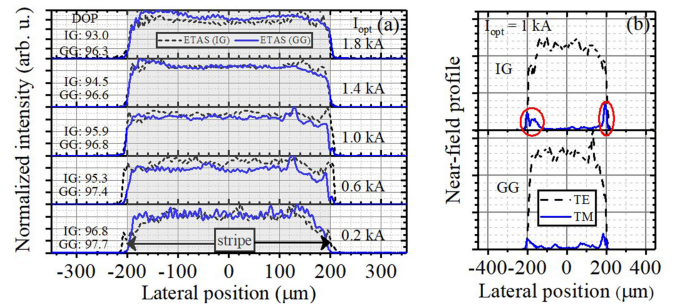

Fig. 9. (a) Near-field distributions along the lateral direction of one of the center (emitter 15) emitters of the gain-guided (solid) and index-guided (dashed) ETAS bars presented in Figs. 7, 8 at different I_{opt} at $T_{HS} = 25$ °C. Degree of polarization (DOP) values are also noted. Shadowed region indicates the active stripe width of the emitter. (b) Polarization-resolved near-field profiles of the center emitters at 1 kA. Circles emphasize the enhancement of TM-polarized emission due to the index-guiding trenches. TM/TE: transverse magnetic/electric.

all emitters, weighted by the relative power level. All near and far field measurements are conducted at low heat levels (200 μs, 10 Hz). We obtain similar trends to earlier papers with lower (2–3°) overall far-fields when IGs are omitted. The near field is shown in Fig. 9(a) for one exemplary emitter, which remains close to the contact width up to 1.8 kA.

Another prominent advantage of the gain-guided ETAS bars is observed in the improvement of the degree of polarization (DOP) which is defined as the fraction of the electrically polarized total

power emitted along bars' base plane. Integrated DOP values for the whole bar are noted in Fig. 9(a). Fig. 9(b) presents the polarization-resolved near-field profiles of the exemplary emitter 15 of the IG and GG ETAS bars at $I_{opt} = 1$ kA. As can be seen in Fig. 9(b)(top), the TM-polarized emission is enhanced at the stripe edges of the IG emitters which is associated with the mechanical stress fields originating from the trenches there [18]. The absence of such mechanical stresses in gain-guided ETAS bars improves their DOP by 1–3% up to $I_{opt} = 1.8$ kA. Overall, the beam quality enhancement for GG bars seen in previous studies [11] is shown here to be maintained to 1.8 kA.

IV. CONCLUSION

An improved power bar based on the ETAS epitaxial layer design concept is presented. In comparison to reference ASLOC bars, ETAS bars deliver higher P_{opt} and η_E both at $T_{HS} = 25\,°C$ and $-70\,°C$, attributed to the thin p-WG for the same well depth, Δ_{QW}. An effective approach is found to narrow lateral beam divergence at low heating levels up to 1.8 kA, without sacrificing the PIU performance, by avoiding index-guiding dry-etched trenches in the bar. ETAS bars that contain merely gain-guided emitters show improved DOP by avoiding mechanical stress-induced TM-polarized fields at the stripe edges. Further improvements in the P_{opt} and η_E can be obtained by further optimizing the ETAS structure with high Γg_0 [10] for 25 °C operation and with waveguide containing low Al-composition for $-70\,°C$ operation [7].

ACKNOWLEDGMENT

REFERENCES

[1] S. D. McDougall *et al.*, "Advances in diode laser bar power and reliability for multi-kW disk laser pump sources," *Proc. SPIE*, vol. 11262, 2020, Art. no. 1126206.

[2] P. Crump and G. Tränkle, "A brief history of kilowatt-class diode-laser bars," *Proc. SPIE*, vol. 11301, 2020, Art. no. 113011D.

[3] L. Woods *et al.*, "Ultra-high peak power laser diode arrays with 1kA-class low SWaP drive electronics," *Proc. SPIE*, vol. 11667, 2021, Art. no. 1166703.

[4] Y. Zhao *et al.*, "High efficiency 1.9 kW single diode laser bar epitaxially stacked with a tunnel junction," *IEEE Photon. J.*, vol. 13, no. 3, Jun. 2021, Art. no. 1500708.

[5] H. Wenzel *et al.*, "Internally wavelength stabilized 910 nm diode lasers with epitaxially stacked multiple active regions and tunnel junctions," *Electron. Lett.*, vol. 58, no. 3, pp. 121–123, 2022.

[6] P. Crump *et al.*, "Cryolaser: Innovative cryogenic diode laser bars optimized for emerging ultra-high power laser applications," in *Proc. Conf. Laser Electro-Opt.*, San Jose, CA, USA, 2013, pp. 1–2, Art. no. JW1J.2.

[7] C. Frevert, "Optimization of broad-area GaAs diode lasers for high powers and high efficiencies in the temperature range 200-220 K," Ph.D. dissertation, Tech. Univ. Berlin, Cuvillier Verlag, Göttingen, Germany, 2018.

[8] K. H. Hasler *et al.*, "Comparative theoretical and experimental studies of two designs of the high-power diode lasers," *Semicond. Sci. Technol.*, vol. 29, no. 4, 2014, Art. no. 045010.

[9] A. Boni, S. Arslan, G. Erbert, P. Della Casa, D. Martin, and P. Crump, "Epitaxial design progress for high power, efficiency, and brightness in 970 nm broad area lasers," *Proc. SPIE*, vol. 11668, 2021, Art. no. 1166807.

[10] T. Kaul, G. Erbert, A. Maaßdorf, S. Knigge, and P. Crump, "Suppressed power saturation due to optimized optical confinement in 9xx nm high-power diode lasers that use extreme double asymmetric vertical designs," *Semicond. Sci. Technol.*, vol. 33, no. 3, 2018, Art. no. 035005.

[11] M. M. Karow, D. Martin, P. Della Casa, G. Erbert, and P. Crump, "Narrower far field and higher efficiency in 1 kW diode-laser bars using improved lateral structuring," in *Proc. Conf. Lasers Electro-Opt. Europe Eur. Quantum Electron. Conf.*, Munich, Germany, 2019, pp. 1–1.

[12] A. Boni, P. Della Casa, D. Martin, and P. Crump, "Efficiency optimization of high-power GaAs lasers by balancing confinement and threshold," in *Proc. 27th Int. Semicond. Laser Conf.*, Potsdam, Germany, 2021, pp. 1–2, Art. no. TuP2.3.

[13] M. M. Kaorw, D. Martin, P. Della Casa, G. Erbert, and P. Crump, "Design progress for higher efficiency and brightness in 1kW diode-laser bars," *Proc. SPIE*, vol. 11262, 2020, Art. no. 1126205.

[14] W. Pittroff *et al.*, "Mounting of high power laser diodes on boron nitride heat sinks using optimized Au/Sn metallurgy," *IEEE Tran. Adv. Packag.*, vol. 24, no. 4, pp. 434–441, Nov. 2001.

[15] M. M. Karow *et al.*, "Long resonator laser-diode bars for efficient kW emission," in *Proc. Eur. Conf. Lasers Electro-Opt.*, 2017, pp. 1–1.

[16] C. Frevert, F. Bugge, S. Knigge, A. Ginolas, G. Erbert, and P. Crump, "940 nm QCW diode laser bars with 70% efficiency at 1 kW output power at 203 K," *Proc. SPIE*, vol. 9733, 2016, Art. no. 97330L.

[17] P. Crump *et al.*, "Efficient high-power laser diodes," *IEEE J. Sel. Top. Quant. Electron.*, vol. 19. no. 4, Jul./Aug. 2013, Art. no. 1501211.

[18] P. Crump *et al.*, "Experimental studies into the beam parameter product of GaAs high-power diode lasers," *IEEE J. Sel. Top. Quant. Electron.*, vol. 28, no. 1, Jan.–Feb. 2022, Art. no. 1501111.